

# SwarmPRM: Probabilistic Roadmap Motion Planning for Swarm Robotic Systems

Yunze Hu<sup>1</sup>, Xuru Yang<sup>1</sup>, Kangjie Zhou<sup>1</sup>, Qinghang Liu<sup>1</sup>, Kang Ding<sup>1</sup>, Han Gao<sup>1</sup>,  
Pingping Zhu<sup>2</sup>, and Chang Liu<sup>1</sup>

**Abstract**—Swarm robotic systems consisting of large-scale cooperative agents hold promise for performing autonomous tasks in diverse fields. However, existing planning strategies for swarm robotic systems often encounter a trade-off between scalability and solution quality. We introduce here SwarmPRM, a hierarchical, highly scalable, computationally efficient, and risk-aware sampling-based motion planning approach for swarm robotic systems, which is asymptotically optimal under mild assumptions. We employ probability density functions (PDFs) to represent the swarm’s macroscopic state and utilize optimal mass transport (OMT) theory to measure the swarm’s cost to go. A risk-aware Gaussian roadmap is constructed wherein each node encapsulates a distinct PDF and conditional-value-at-risk (CVaR) is employed to assess the collision risk, facilitating the generation of macroscopic PDFs in Wasserstein–GMM space. Extensive simulations demonstrate that the proposed approach outperforms state-of-the-art methods in terms of computational efficiency and the average travelling distance.

## I. INTRODUCTION

With the development of low-cost sensors, communication and computational systems, swarm robotic systems comprised of large-scale autonomous robots are becoming a viable solution for executing autonomous tasks across various domains, such as exploration of unknown environments [1], search and rescue [2], and swarm coordination [3].

Significant advancements have been achieved in the field of multi-agent optimal control [4, 5], aiming at controlling the agents in an optimal manner and minimizing a global cost function while adhering to dynamics and safety constraints. However, the scalability is relatively poor and is practically limited in the order of several dozens robots. Alternatively, the swarm robotic approach has been proposed [6, 7] to facilitate the designation of scalable and distributed control strategies in swarm robotic systems. The mean-field models [6] have been employed to characterize the collective behaviors of the swarm using a time-evolving probability density function (PDF), and the PDF dynamics is governed by the evolution partial differential equations (PDEs). Notably, the employment of optimal mass transport (OMT) theory to

guide density control [7] offers a natural framework for minimizing swarm deployment costs.

The hierarchical framework has demonstrated effectiveness in addressing scalability and computational efficiency challenges in swarm robotic systems. Alonso-Mora et al. [8] developed a multi-robot formation control algorithm integrating a global path planner for formation navigation with a local motion planner for online optimization and robot control. However, such an approach mandates swarm robots to maintain specific formations, which is neither necessary in various practical scenarios nor scalable to large-scale swarm robotic systems. Rudd et al. [9] employed PDFs to represent the macroscopic states of the swarm robotic system and calculated the optimal robot distribution at each time step, which provided guidance for the designation of the optimal robot microscopic actions. Zhu et al. [10] utilized the OMT theory to plan the optimal time-varying robot PDFs, and efficiently tackled the swarm optimal control problem in complex environments by devising solutions within the Wasserstein-Gaussian mixture model (GMM) space. Despite the progress made, the solutions are found based on a series of numerical implementations, and thus have no optimality guarantee.

Collision avoidance is of great importance in motion planning of swarm robotic systems to ensure safety, and various risk measures can be utilized for collision checking. Zhu and Alonso-Mora [11] utilized chance constraints to ensure the collision probability between each mobile robot and obstacle is below a user-specified threshold during navigation. On the other hand, the conditional value at risk (CVaR) is a risk measure quantifying the potential losses beyond a certain confidence level. CVaR has gained significant attention in the robotics community [12, 13]. In contrast to its widely-used counterpart, chance constraints, CVaR takes into account the tail distribution through conditional expectation, which enables the discerning of rare events. Furthermore, CVaR is coherent in the sense of Artzner et al. [14], as opposed to chance constraints, and is advocated as a rational risk measure in robotics applications.

The sampling-based motion planning approach has gained considerable popularity in efficiently solving motion planning problems in complex environments. Karaman and Frazzoli [15] proposed PRM\* and RRT\* that have strong theoretical properties, probabilistic completeness and asymptotic optimality, and remarkable practical performance. Čáp et al. [16] adapted RRT\* to solve the multi-agent motion planning problem in a centralized manner, through treating the union

<sup>1</sup>Yunze Hu, Xuru Yang, Kangjie Zhou, Qinghang Liu, Kang Ding, Han Gao, and Chang Liu are with the Department of Advanced Manufacturing and Robotics, College of Engineering, Peking University, Beijing 100871, China (hu\_yun\_ze@stu.pku.edu.cn; xuru.yang@stu.pku.edu.cn; kangjiezhou@pku.edu.cn; californium@stu.pku.edu.cn; kangding@stu.pku.edu.cn; hangao-coe@pku.edu.cn; changliucoe@pku.edu.cn). All correspondences should be sent to Chang Liu.

<sup>2</sup>Pingping Zhu is with the Department of Computer Sciences and Electrical Engineering (CSEE), Marshall University, Huntington, WV 25755, USA (zhup@marshall.edu).

of all the agents as a single system, but this approach is computationally intractable due to the exponential growth of the search space. Hönl et al. [17] increased the scalability by first generating a sparse roadmap and then utilizing multi-agent path finding approaches to perform discrete planning subject to interrobot constraints. Shome et al. [18] proposed dRRT\*, an informed, asymptotically optimal sampling-based algorithm including construction of roadmaps for each robot and implicit search without requiring an explicit representation of the joint motion graph. Nevertheless, a trade-off has to be made between scalability and optimality guarantee, when employing state-of-the-art sampling-based motion planning approaches [17, 18].

In light of these gaps, we propose SwarmPRM, a hierarchical, highly scalable, computationally efficient, and risk-aware sampling-based motion planning approach for swarm robotic systems, which is asymptotically optimal under mild assumptions. At the macroscopic level, the collective swarm is presented by a time-varying PDF, while at the microscopic level, the optimal control law is determined to direct individual robots in tracking the macroscopic PDF. The main contributions of this work are threefold:

- 1) We propose the SwarmPRM algorithm for motion planning of swarm robotic systems. Specifically, we construct a Gaussian roadmap to facilitate the generation of the macroscopic PDF in Wasserstein–GMM space. Furthermore, we establish the asymptotic optimality of SwarmPRM for planning the time-varying PDF under mild assumptions.
- 2) We employ CVaR to evaluate the collision risk between the swarm robotic system and environmental obstacles. Detailedly, we model the SDF between the swarm and obstacles as a probability distribution, and calculate CVaR of the SDF distribution to quantify the collision risk.
- 3) Through extensive simulations, we demonstrate the superiority of our SwarmPRM algorithm over other state-of-the-art approaches in aspects of computational efficiency and average travelling distance. Furthermore, our algorithm exhibits scalability to swarm robotic systems comprising hundreds of robots.

## II. PROBLEM FORMULATION AND BACKGROUND

### A. Hierarchical Planning Strategy for Swarm Robotics

Consider a swarm robotic system represented by the set  $\mathcal{R} = \{1, 2, \dots, N\}$ , where  $N$  denotes the total number of homogeneous robots, within a large two-dimensional cluttered environment  $\mathcal{W}$  containing  $N_{Obs}$  obstacles  $\mathcal{O} = \{\mathcal{O}_1, \dots, \mathcal{O}_{N_{Obs}}\}$ . The objective is to devise trajectories for all robots, directing them from initial positions to target areas. The obstacles are static and known a priori, and under the assumptions of connectivity and information sharing, the states of the robots are fully observable. The initial positions of the robots in the swarm are denoted as  $\mathcal{Q} = \{q_1, \dots, q_N\}$ , and the dynamics are modeled by a stochastic differential equation.

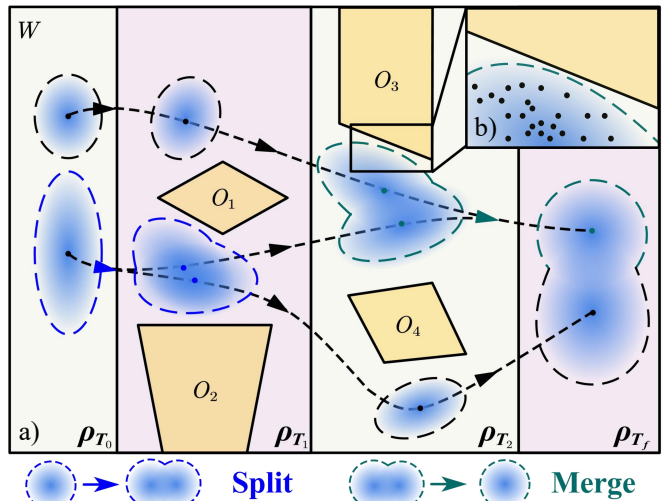


Fig. 1: **(a) The macroscopic planning of the swarm robotic system.** The macroscopic state of the swarm is represented by a time-varying PDF. In the two-dimensional cluttered environment  $\mathcal{W}$ , the obstacles  $\mathcal{O}_1, \mathcal{O}_2, \mathcal{O}_3, \mathcal{O}_4$  are coloured in light orange, and the macroscopic PDF is represented in blue colour, with darker shades indicating higher probabilities, and coloured dotted lines delineating the  $\alpha$ -confidence area, where  $\alpha$  is a preset parameter. The optimal PDF transport trajectory, represented by the black dotted lines and coloured arrows, guides the swarm macroscopic state from the initial distribution  $\rho_{T_0}$  to the target distribution  $\rho_{T_f}$ , with two PDFs  $\rho_{T_1}$  and  $\rho_{T_2}$  denoting the swarm's intermediate macroscopic states along the trajectory. Optimal transport may involve "splitting" or "merging" maneuvers, depicted by the blue and green dotted lines and arrows, respectively. **(b) The microscopic state of robots in the swarm.** Each black dot signifies a robot positioned within the  $\alpha$ -confidence area and maintains collision-free movement with respect to obstacles, showcasing the necessity of the collision avoidance constraint at the macroscopic level.

We adopt a hierarchical motion planning strategy for the swarm robotic system (Fig. 1). At the macroscopic level, the entirety of the swarm is represented by a time-varying PDF  $\chi(\mathbf{x}, t) \in \mathcal{P}(\mathcal{W})$ , where  $\mathbf{x} \in \mathcal{W}$ ,  $\mathcal{P}(\mathcal{W})$  is the space of PDFs with support  $\mathcal{W}$  [9], and  $t$  denotes the time. Subsequently, at the microscopic level, optimal controls are calculated to guide each robot in tracking the macroscopic PDF trajectory while ensuring collision avoidance with obstacles and other robots.

In the macroscopic planning stage, the swarm is tasked with transitioning from a given initial distribution  $\chi(\mathbf{x}, T_0) \triangleq \rho_{T_0}$  to a desired distribution  $\chi(\mathbf{x}, T_f) \triangleq \rho_{T_f}$  while simultaneously avoiding obstacles. The optimal macroscopic PDF transport trajectory  $\chi(\mathbf{x}, t)$  can be calculated by solving the following optimization problem

$$\min_{\chi} J(\chi(\mathbf{x}, t)) \quad (1)$$

$$\text{s.t. } \rho_{T_0} = \chi(\mathbf{x}, T_0), \quad (1a)$$

$$\rho_{T_f} = \chi(\mathbf{x}, T_f), \quad (1b)$$

$$R_{\alpha}(\chi(\mathbf{x}, t)) \leq \delta, \forall t \in [T_0, T_f], \quad (1c)$$

where (1a), (1b) represent the swarm's initial and target macroscopic PDF state, respectively, and (1c) is the collision

avoidance constraint, which will be detailed in Sec. III-B. The objective is to minimize the swarm's transport distance  $J$ , while adhering to the aforementioned constraints.

### B. Sampling-Based Motion Planning Algorithms

Sampling-based Algorithms (SBAs) have been a prevalent strategy for motion planning in robotics [15, 19, 20], characterized by a triplet  $(\mathcal{X}_{free}, \mathbf{x}_{init}, \mathbf{x}_{goal})$ , where  $\mathcal{X}_{free}$ ,  $\mathbf{x}_{init}$ , and  $\mathbf{x}_{goal}$  represent the collision-free configuration space, the initial configuration, and the goal configuration, respectively. The objective is to find a collision-free trajectory  $\varphi : [0, 1] \rightarrow \mathcal{X}_{free}$ , satisfying  $\varphi(0) = \mathbf{x}_{init}$  and  $\varphi(1) = \mathbf{x}_{goal}$ . SBAs operate by randomly sampling the configuration space and constructing a tree or graph, which expresses the connectivity and the feasible paths within the space. In this work, we specifically consider PRM and PRM\* [15]. Initially, new samples are randomly drawn from the collision-free configuration space  $\mathcal{X}_{free}$  to create graph nodes in the roadmap. Subsequently, each node in the graph undergoes a query process to identify neighboring nodes to which the transition is collision-free with respect to obstacles, and edges connecting the respective nodes are added to the probabilistic roadmap.

### C. Optimal Transport Theory and Wasserstein Metrics

The OMT theory [21], originating from Gaspard Monge's work in 1781, tackles the task of transporting masses from an initial distribution to a terminal one while maintaining mass continuity and minimizing associated costs. The Wasserstein distance  $W_2$ , derived from the minimal transport cost within the space of PDFs, not only demonstrates crucial metric properties but also holds significant physical interpretations.

Let  $v_1, v_2 \in \mathcal{P}(\mathcal{W})$  denote two PDFs with support  $\mathcal{W}$ . Define  $\Pi(v_1, v_2) \subset \mathcal{P}(\mathcal{W} \times \mathcal{W})$  as the set that comprises all joint PDFs characterized by marginal measures along the two coordinate directions that align with  $v_1$  and  $v_2$ , respectively, and the Wasserstein metric is defined as

$$W_2(v_1, v_2) \triangleq \left[ \inf_{\pi \in \Pi(v_1, v_2)} \int_{\mathcal{W} \times \mathcal{W}} \|\mathbf{x}_1 - \mathbf{x}_2\|_2^2 d\pi(\mathbf{x}_1, \mathbf{x}_2) \right]^{\frac{1}{2}}, \quad (2)$$

where  $\|\cdot\|_2$  represents the Euclidean distance.

The Wasserstein metric between two Gaussian distributions  $g_1 \sim \mathcal{N}(\boldsymbol{\mu}_1, \Sigma_1), g_2 \sim \mathcal{N}(\boldsymbol{\mu}_2, \Sigma_2)$  can be calculated as follows,

$$W_2(g_1, g_2) = \left\{ \|\boldsymbol{\mu}_1 - \boldsymbol{\mu}_2\|^2 + \text{tr} \left[ \Sigma_1 + \Sigma_2 - 2(\Sigma_1^{\frac{1}{2}} \Sigma_2 \Sigma_1^{\frac{1}{2}})^{\frac{1}{2}} \right] \right\}^{\frac{1}{2}}, \quad (3)$$

where  $\text{tr}(\cdot)$  represents the trace of a matrix. The geodesic path  $\hat{g}_{1,2}(t), t \in [0, 1]$  between  $g_1$  and  $g_2$  is also Gaussian with mean

$$\hat{\boldsymbol{\mu}}(t) = (1-t)\boldsymbol{\mu}_1 + t\boldsymbol{\mu}_2 \quad (4)$$

and covariance

$$\hat{\Sigma}(t) = \Sigma_1^{-\frac{1}{2}} \left[ (1-t)\Sigma_1 + t(\Sigma_1^{\frac{1}{2}} \Sigma_2 \Sigma_1^{\frac{1}{2}})^{\frac{1}{2}} \right]^2 \Sigma_1^{-\frac{1}{2}}. \quad (5)$$

While the Wasserstein metric between two Gaussian distributions can be analytically calculated, there is currently no efficient representation for general distributions [22]. A new metric in the space of all Gaussian Mixture Models (GMMs),  $\mathcal{GM}(\mathcal{W})$ , defined as

$$D(\varrho_1, \varrho_2) = \left\{ \min_{\pi \in \Pi(\boldsymbol{\omega}_1, \boldsymbol{\omega}_2)} \sum_{i=1}^{N_1} \sum_{j=1}^{N_2} \left[ W_2(g_1^i, g_2^j) \right]^2 \pi(i, j) \right\}^{\frac{1}{2}}, \quad (6)$$

has been proposed in [21] as an efficient approximation to the Wasserstein metric for any two GMMs  $\varrho_1 = \sum_{i=1}^{N_1} \omega_1^i g_1^i, \varrho_2 = \sum_{j=1}^{N_2} \omega_2^j g_2^j \in \mathcal{GM}(\mathcal{W})$ , where  $\boldsymbol{\omega}_1 = [\omega_1^1, \dots, \omega_1^{N_1}]$  and  $\boldsymbol{\omega}_2 = [\omega_2^1, \dots, \omega_2^{N_2}]$  are associated weight vectors satisfying  $\sum_{i=1}^{N_1} \omega_1^i = 1, \sum_{j=1}^{N_2} \omega_2^j = 1$ . The geodesic path connecting  $\varrho_1$  and  $\varrho_2$  is given by

$$\hat{\varrho}_{1,2}(t) = \sum_{i,j} \pi^*(i, j) \hat{g}_{1,2}^{i,j}(t), t \in [0, 1], \quad (7)$$

where  $\pi^*(i, j)$  is the optimal joint distribution defined in Eq. (6), and  $\hat{g}_{1,2}^{i,j}(t)$  represents the displacement interpolation between Gaussian distributions  $g_1^i$  and  $g_2^j$ , which can be calculated based on Eq. (4) and Eq. (5).

### D. Conditional Value at Risk

Given a PDF  $v(x)$  and a risk parameter  $\alpha$ , the CVaR calculates the conditional expectation of the loss within the  $1 - \alpha$  worst-case quantile [12]. The CVaR of an Gaussian distribution  $v \sim \mathcal{N}(\mu, \sigma^2)$  with risk parameter  $\alpha$  is derived as

$$\text{CVaR}_\alpha(v) = \mathbb{E}[\psi | \psi \geq \text{VaR}_\alpha(v)] = \mu + \frac{\phi(\Phi^{-1}(1 - \alpha))}{\alpha} \sigma, \quad (8)$$

where  $\phi$  and  $\Phi$  are the PDF and cumulative density function (CDF) of the standard normal distribution, respectively.

## III. CONSTRUCTION OF RISK-AWARE GAUSSIAN ROADMAP

The swarm's macroscopic state is represented by a time-varying PDF  $\chi(\mathbf{x}, t), t \in [T_0, T_f]$ . The GMM is a universal approximator of probability densities [23], so without loss of generality, we approximate the time-varying PDF  $\chi(\mathbf{x}, t)$  as GMMs. The swarm's initial and target macroscopic states are modeled as two GMMs  $\varrho_{T_0}, \varrho_{T_f}$ , and the optimal PDF transport trajectory is devised in GMM space  $\mathcal{GM}$ , i.e.,  $\forall t \in [T_0, T_f], \chi(\mathbf{x}, t) \in \mathcal{GM}, \chi(\mathbf{x}, T_0) = \varrho_{T_0}, \chi(\mathbf{x}, T_f) = \varrho_{T_f}$ . The distance metric Eq. (6) and the corresponding geodesic Eq. (7) in GMM space suggest that the optimal transport between two GMMs can be achieved through transport weight allocation between their respective Gaussian components. Furthermore, the geodesic path Eq. (4) and Eq. (5) between two Gaussian distributions imply that each intermediate state along the optimal transport trajectory between two Gaussian distributions retains a Gaussian distribution. Therefore, we assume that the optimal transport trajectory can be achieved through a set of Gaussian distribution trajectories originating from the Gaussian components of  $\varrho_{T_0}$  and converging towards those of  $\varrho_{T_f}$ .

Inspired by PRM, we develop a sampling-based motion planning approach and construct a Gaussian roadmap at the macroscopic planning stage. Each node in the roadmap represents a Gaussian distribution, and the cost between two nodes is determined by the Wasserstein metric. The objective is to plan the optimal Gaussian distribution trajectories and calculate the associated costs between Gaussian components of  $\varrho_{T_0}$  and  $\varrho_{T_f}$ , facilitating the calculation of the optimal GMM trajectory  $\chi(\mathbf{x}, t)$  between  $\varrho_{T_0}$  and  $\varrho_{T_f}$ , which will be detailed in Sec. IV.

### A. Roadmap Construction

Denote  $\mathcal{G}$  as the space of Gaussian distributions, where each element is a 2-dimensional Gaussian distribution denoted as  $g \sim \mathcal{N}(\boldsymbol{\mu}, \Sigma)$ , with the mean  $\boldsymbol{\mu} \in \mathcal{W}$ , and covariance matrix  $\Sigma$  satisfying<sup>1</sup>

$$\Sigma = \begin{bmatrix} \sigma_1^2 & \rho\sigma_1\sigma_2 \\ \rho\sigma_1\sigma_2 & \sigma_2^2 \end{bmatrix}, \quad (9)$$

$$0 < \sigma_{lb} \leq \sigma_1, \sigma_2 \leq \sigma_{ub}, \quad (10)$$

$$-1 < \rho_{lb} \leq \rho \leq \rho_{ub} < 1. \quad (11)$$

We utilize five-dimensional parameter vectors  $\mathbf{v} = [x, y, \sigma_1, \sigma_2, \rho]$  to represent Gaussian distributions in  $\mathcal{G}$ , with mean  $[x, y]$  and covariance matrix in the form of (9). The parameter vectors form a parameter space  $\mathcal{X} \subset \mathbb{R}^5$ , which is in essence an Euclidean space. We can build a bijection  $h$  between the parameter space  $\mathcal{X}$  and the space of Gaussian distributions  $\mathcal{G}$ , i.e.,  $h : \mathcal{X} \rightarrow \mathcal{G}$ , and  $h^{-1} : \mathcal{G} \rightarrow \mathcal{X}$ , and define a cost function  $c : \mathcal{X} \times \mathcal{X} \rightarrow \mathbb{R}$  based on the Wasserstein metric, i.e.,  $\forall \mathbf{v}_i, \mathbf{v}_j \in \mathcal{X}, c(\mathbf{v}_i, \mathbf{v}_j) = W_2(h(\mathbf{v}_i), h(\mathbf{v}_j))$ . Denote  $T$  as the set of all paths  $\tau$  in the parameter space, and the function  $L : T \rightarrow \mathbb{R}_{\geq 0}$  as the cost function [15]. Based on the definition of the total variation [15], the cost of a path  $\tau$  in parameter space  $\mathcal{X}$  is derived as  $L(\tau) \triangleq \sup_{n \in \mathbb{N}, 0 = \iota_0 < \dots < \iota_n = 1} \sum_{i=1}^n c(\tau(\iota_i) - \tau(\iota_{i-1}))$ . The objective of constructing the Gaussian roadmap is to plan the collision-free path with minimal cost in the parameter space  $\mathcal{X}$  between each pair of Gaussian distributions, and thus calculate the optimal PDF transport trajectory in Wasserstein-Gaussian space  $(\mathcal{G}, W_2)$ .

The roadmap construction approach (Alg. 1) is outlined in the ROADMAPCONSTRUCTION function, which takes the number of samples  $n$ , the connection radius  $r_n$ , the set of obstacles  $\mathcal{O}$ , and a set  $\mathcal{D}$  representing the set of initial and target PDFs as inputs. Initially, a node set  $V$  is constructed in parameter space  $\mathcal{X}$  through the combination of the set  $h^{-1}(\mathcal{D}) \subset \mathcal{X}$  as well as  $n \in \mathbb{N}$  nodes in free space generated by the function SAMPLEFREE (Line 1). Subsequently, for each node  $\mathbf{v} \in V$ , the function NEAR calculates the set  $X_{near}$  containing all nodes located in the neighbourhood of node  $\mathbf{v}$  (Line 4). For each node  $\mathbf{v}' \in X_{near}$ , the edges  $(\mathbf{v}, \mathbf{v}')$

<sup>1</sup>Note that the constraints (10) and (11) are mild assumptions that are used to ensure the covariance matrix remains nonsingular, while at the same time upholding the property of asymptotic optimality of our approach. The removal of these constraints will not alter the overall framework of our approach.

---

### Algorithm 1: Gaussian Roadmap Construction

---

```

Procedure ROADMAPCONSTRUCTION( $n, r_n, \mathcal{O}, \mathcal{D}$ )
1:  $V \leftarrow h^{-1}(\mathcal{D}) \cup \text{SAMPLEFREE}(n, \mathcal{O}); E \leftarrow \emptyset$ 
2: for  $\mathbf{v} \in V$  do
3:   Map  $\mathbf{v}$  to  $g_{\mathbf{v}} \sim \mathcal{N}_{\mathbf{v}}(\boldsymbol{\mu}, \Sigma)$  using  $h$ 
4:    $X_{near} \leftarrow \text{NEAR}(V \setminus \{\mathbf{v}\}, \mathbf{v}, r_n)$ 
5:   for  $\mathbf{v}' \in X_{near}$  do
6:     Map  $\mathbf{v}'$  to  $g_{\mathbf{v}'} \sim \mathcal{N}_{\mathbf{v}'}(\boldsymbol{\mu}, \Sigma)$  using  $h$ 
7:     if COLLISIONFREE( $g_{\mathbf{v}}, g_{\mathbf{v}'}, \mathcal{O}$ ) and  $\hat{g}_{\mathbf{v}, \mathbf{v}'} \in \mathcal{G}$  then
8:        $E \leftarrow E \cup \{(\mathbf{v}, \mathbf{v}')\} \cup \{(\mathbf{v}', \mathbf{v})\}$ 
9:     end if
10:  end for
11: end for
12: return  $G = (V, E)$ 

Procedure SAMPLEFREE( $n, \mathcal{O}$ )
13:  $V \leftarrow \emptyset$ 
14: while  $|V| < n$  do
15:   Generate random sample  $\mathbf{v} \in \mathcal{X}$ 
16:   Map  $\mathbf{v}$  to  $g_{\mathbf{v}} \sim \mathcal{N}_{\mathbf{v}}(\boldsymbol{\mu}, \Sigma)$  using  $h$ 
17:   if INFREE( $g_{\mathbf{v}}, \mathcal{O}$ ) then
18:      $V \leftarrow V \cup \{\mathbf{v}\}$ 
19:   end if
20: end while
21: return  $V$ 

Procedure NEAR( $V', \mathbf{v}, r_n$ )
22:  $X_{near, i} \leftarrow \emptyset$ 
23: for  $\mathbf{v}' \in V'$  do
24:   if  $c(\mathbf{v}, \mathbf{v}') \leq r_n$  then
25:      $X_{near, i} \leftarrow X_{near, i} \cup \{\mathbf{v}'\}$ 
26:   end if
27: end for
28: return  $X_{near, i}$ 

Procedure INFREE( $g, \mathcal{O}$ )
29: for all obstacle  $\mathcal{O} \in \mathcal{O}$  do
30:   Calculate SDF between  $g$  and  $\mathcal{O}$  using (14)
31:   if (15) not holds then
32:     return false
33:   end if
34: end for
35: return true

```

---

and  $(\mathbf{v}', \mathbf{v})$  are added to the edge set  $E$ , if the geodesic path between the corresponding two Gaussian distributions  $g_{\mathbf{v}} = h(\mathbf{v})$  and  $g_{\mathbf{v}'} = h(\mathbf{v}')$ , defined based on the Wasserstein metric, is a subset of the obstacle-free region in  $\mathcal{G}$  (Line 3, 5-8). Finally, a graph  $G = (V, E)$  is constructed (Line 12). The main functions SAMPLEFREE and NEAR are detailed as follows, and the functions INFREE and COLLISIONFREE will be detailed in Sec. III-B.

1) SAMPLEFREE: The function SAMPLEFREE( $n$ ) returns a set of  $n \in \mathbb{N}$  nodes in free space. Whenever the number of nodes in the set  $V$  is less than  $n$ , a random sample  $\mathbf{v}$  is generated in parameter space  $\mathcal{X}$  (Line 15-16). If the corresponding Gaussian distribution  $g_{\mathbf{v}} = h(\mathbf{v})$  is in free space, as verified by the function INFREE, then the node  $\mathbf{v}$  is added to the set  $V$  (Line 17-19). We consider a generic form of the PRM algorithm, and various sampling strategies, including random sampling and deterministic sampling methods [20], can be chosen to sample  $\mathbf{v}$ .

2) NEAR: The function NEAR takes the node  $\mathbf{v}$ , connection radius  $r_n$ , and the node set  $V'$  as inputs, and returns the set  $X_{near, i} \subset V'$  containing all nodes located in the neighbourhood of node  $\mathbf{v}$ . For each node  $\mathbf{v}'$  in the set  $V'$ , if

$c(\mathbf{v}, \mathbf{v}')$  is no more than the connection radius  $r_n$ , then  $\mathbf{v}'$  is added to the set  $X_{near,i}$  (Line 25-27).

### B. Collision Detection Based on CVaR

We utilize a risk assessment metric, CVaR, to conduct collision detection between a Gaussian distribution representing the swarm robots' macroscopic state and an obstacle  $\mathcal{O}$ , ensuring that the collision risk does not exceed a manually specified risk threshold  $\alpha$ . Consider a robot team whose macroscopic state can be represented by a Gaussian distribution. Through linearization, we can model the probabilistic distribution of the swarm's signed distance function (SDF) as a Gaussian distribution. Subsequently, we utilize CVaR to constrain the conditional expectation of the SDF within the  $1 - \alpha$  worst-case quantile to reside within the safe region, where  $\alpha$  is a risk parameter.

1) *SDF Linearization and CVaR Collision Detection:* The SDF quantifies the distance between two sets  $\mathcal{A}$  and  $\mathcal{B}$ ,

$$s(\mathcal{A}, \mathcal{B}) = \begin{cases} \inf\{\|\mathbf{t}\|_2 \mid \mathbf{t} + \mathcal{A} \cap \mathcal{B} \neq \emptyset\}, & \text{if } \mathcal{A} \cap \mathcal{B} = \emptyset, \\ -\inf\{\|\mathbf{t}\|_2 \mid \mathbf{t} + \mathcal{A} \cap \mathcal{B} = \emptyset\}, & \text{if } \mathcal{A} \cap \mathcal{B} \neq \emptyset, \end{cases} \quad (12)$$

which can be calculated utilizing Gilbert–Johnson–Keerthi (GJK) algorithm for non-intersecting sets and Expanding Polytope Algorithm (EPA) for overlapping shapes [24]. For deterministic point  $\mathbf{p}$  and obstacle  $\mathcal{O}$ , we can obtain the signed distance  $\hat{d} \in \mathbb{R}$ , the closest points from the obstacle  $\mathbf{p}_{\mathcal{O}} \in \mathcal{O}$ , and the contact normal  $\mathbf{n}(\mathbf{p}, \mathcal{O}) = \text{sgn}(\hat{d})(\mathbf{p}_{\mathcal{O}} - \mathbf{p})/\|\mathbf{p}_{\mathcal{O}} - \mathbf{p}\|$ .

For a stochastic point  $\mathbf{p} \sim \mathcal{N}(\boldsymbol{\mu}, \Sigma)$  and deterministic obstacle  $\mathcal{O}$ , the SDF can be linearized as

$$s(\mathbf{p}, \mathcal{O}) \approx s(\boldsymbol{\mu}, \mathcal{O}) + \nabla s(\mathbf{p}, \mathcal{O})|_{\mathbf{p}=\boldsymbol{\mu}} \cdot (\mathbf{p} - \boldsymbol{\mu}), \quad (13)$$

which approximates the obstacle area as a half plane with outer normal vector  $-\mathbf{n}(\boldsymbol{\mu}, \mathcal{O})$ , so that  $\nabla s(\mathbf{p}, \mathcal{O})|_{\mathbf{p}=\boldsymbol{\mu}} = \mathbf{n}(\boldsymbol{\mu}, \mathcal{O}) \triangleq \mathbf{n}$ . It is obvious that the random variable  $s(\mathbf{p}, \mathcal{O})$  satisfies a Gaussian distribution with mean  $s(\boldsymbol{\mu}, \mathcal{O})$  and covariance  $\mathbf{n}^T \Sigma \mathbf{n}$  [13, 24].

2) *CVaR Collision Detection for Swarm Robotic Systems:* Given a team of robots whose macroscopic state is represented by a Gaussian distribution  $g \sim \mathcal{N}(\boldsymbol{\mu}, \Sigma)$  and an obstacle  $\mathcal{O}$ , the SDF  $s(g, \mathcal{O})$  can be approximated as a Gaussian distribution. Denote  $\eta$  as the negation of the SDF,

$$\eta \triangleq -s(\mathcal{N}(\boldsymbol{\mu}, \Sigma), \mathcal{O}) \approx \mathcal{N}(-s(\boldsymbol{\mu}, \mathcal{O}), \mathbf{n}^T \Sigma \mathbf{n}), \quad (14)$$

and a greater value of  $\eta$  indicates a smaller SDF value between the swarm and the obstacle  $\mathcal{O}$ , and  $-s(\mathcal{N}(\boldsymbol{\mu}, \Sigma), \mathcal{O})$  is approximated through (13). We subsequently compute the CVaR of  $\eta$ , and the collision avoidance requirement can be written as

$$\text{CVaR}_{\alpha}(\eta, \mathcal{O}) \leq \delta, \quad (15)$$

where  $\alpha$  denotes the collision risk, and  $\delta \leq 0$  represents the safe region, constraining the conditional expectation of opposite SDF within the  $1 - \alpha$  worst-case quantile to be no more than  $\delta$ . In other words, (15) requires the swarm to be located in the safe region with a minimum percentage of  $1 - \alpha$ .

During the construction of the Gaussian roadmap, the function INFREE serves to check whether the nodes are collision-free with respect to obstacles, as presented in Alg. 1. For a Gaussian distribution  $g$ , all obstacles are queried to calculate the SDF which is a random variable following a Gaussian distribution (Line 32-33). Subsequently, the CVaR is calculated and the function INFREE returns **False** if (15) is not satisfied for a certain obstacle  $\mathcal{O}$  (Line 34-35). Otherwise, the function INFREE returns **True** (Line 38). The function COLLISIONFREE (Line 7) checks whether the transition between two Gaussian distributions  $g_v$  and  $g_{v'}$  is collision-free with respect to obstacles  $\mathcal{O}$ , i.e.,  $\forall g \in \hat{g}_{v,v'}(t), t \in [0, 1], \text{INFREE}(g, \mathcal{O})$  returns **True**. In practical implementation, the collision checking for  $\hat{g}_{v,v'}(t)$  can be achieved approximately by performing INFREE assessments for a collection of Gaussian distributions interpolated between  $g_v$  and  $g_{v'}$  based on Eq. (4) and Eq. (5).

### C. Property Analysis of the Risk-Aware Gaussian Roadmap

We analyze the property of the constructed risk-aware Gaussian roadmap in the parameter space  $\mathcal{X}$ . The proofs of Lemma 1 and Theorem 1 are provided in Appendix I and II, respectively.

**Lemma 1.** *The cost function  $c$  defined based on the Wasserstein metric satisfies: 1) the triangle inequality,  $\forall \mathbf{v}_i, \mathbf{v}_j, \mathbf{v}_k \in \mathcal{X}, c(\mathbf{v}_i, \mathbf{v}_j) + c(\mathbf{v}_j, \mathbf{v}_k) \geq c(\mathbf{v}_i, \mathbf{v}_k)$ , 2) additivity,  $\forall \varphi_1, \varphi_2 : [0, 1] \rightarrow \mathcal{X}, \varphi_1(1) = \varphi_2(0), L(\varphi_1 \varphi_2) = L(\varphi_1) + L(\varphi_2)$ , where  $\varphi_1 \varphi_2$  denotes the concatenation of two paths when  $\varphi_1$  ends at the point at which  $\varphi_2$  begins, and  $L(\varphi) \triangleq \sup_{\mathbf{p} \in \mathbb{N}, 0 = \iota_0 < \dots < \iota_n = 1} \sum_{i=1}^n c(\varphi(\iota_i) - \varphi(\iota_{i-1}))$ , and 3) natural relationship with Euclidean distance in the configuration space,  $\exists \hat{\beta}_1, \hat{\beta}_2 \in (0, \infty), \forall \mathbf{v}_i, \mathbf{v}_j \in [0, 1]^5, \hat{\beta}_1 \|\mathbf{v}_i - \mathbf{v}_j\| \leq c(\mathbf{v}_i, \mathbf{v}_j) \leq \hat{\beta}_2 \|\mathbf{v}_i - \mathbf{v}_j\|$ .*

**Theorem 1.** *The Alg. 1 is asymptotically optimal for planning the PDF transport trajectory between any two Gaussian distributions.*

## IV. HIERARCHICAL FRAMEWORK FOR SWARM PLANNING

Our SwarmPRM approach (Alg. 2) comprises the following two planning stages. At the macroscopic stage (Line 1-9), we leverage the Gaussian roadmap constructed in Sec. III to address the optimal transport problem (1) within the GMM space, thereby guiding the generation of GMM trajectory  $\chi(\mathbf{x}, t)$ . Subsequently, the microscopic control for each robot is calculated to track the macroscopic GMM trajectory (Line 10).

### A. Macroscopic Motion Planning in GMM Space

Consider the macroscopic planning problem in GMM space  $\mathcal{GM} \triangleq \{\varrho \mid \varrho = \sum_{i=1}^k \omega_i g_i, \forall g_i \in \mathcal{G}, k \in \mathbb{N}, \sum_{i \in \mathcal{E}} \omega_i = 1\}$ . Denote the initial and target swarm state as  $\varrho_{T_0} = \chi(\mathbf{x}, T_0) = \sum_{i=1}^{N_1} \omega_{T_0}^i g_{T_0}^i$ , and  $\varrho_{T_f} = \chi(\mathbf{x}, T_f) = \sum_{j=1}^{N_2} \omega_{T_f}^j g_{T_f}^j$ , respectively, where  $\varrho_{T_0}$  comprises  $N_1$  Gaussian components  $\Gamma_{T_0} = \{g_{T_0}^1, \dots, g_{T_0}^{N_1}\}$  with weights  $\omega_{T_0} = [\omega_{T_0}^1, \dots, \omega_{T_0}^{N_1}]$ ,  $\varrho_{T_f}$  consists of  $N_2$

Gaussian components  $\Gamma_{T_f} = \{g_{T_f}^1, \dots, g_{T_f}^{N_2}\}$  with weights  $\omega_{T_f} = [\omega_{T_f}^1, \dots, \omega_{T_f}^{N_2}]$ . Building upon the discussions in Sec. III, we assume that the optimal transport between  $\varrho_{T_0}$  and  $\varrho_{T_f}$  can be achieved through  $K$  Gaussian trajectories  $\Xi = \{\xi_1(\mathbf{x}, t), \dots, \xi_K(\mathbf{x}, t), t \in [T_0, T_f]\}$  satisfying  $\forall t \in [T_0, T_f], \forall i \in \{1, \dots, K\}, \xi_i(\mathbf{x}, t) \in \mathcal{G}$ . Here the number of PDF trajectories  $K$ , as an optimization variable, is limited to be no greater than the number of swarm robots, i.e.,  $K \leq N$ . Denote  $\Lambda$  as  $\{\lambda_1, \dots, \lambda_K\}$ , indicating the percentage of robots in the swarm following each Gaussian trajectory, with  $\sum_{i=1}^K \lambda_i = 1$ . Each trajectory  $\xi_i(\mathbf{x}, t)$  is weighted by  $\lambda_i \in \Lambda$  to satisfy the normalization property of the swarm macroscopic GMM  $\chi(\mathbf{x}, t)$ , so that  $\forall t \in [T_0, T_f], \chi(\mathbf{x}, t) = \sum_{i=1}^K \lambda_i \xi_i(\mathbf{x}, t)$ . Note that different Gaussian trajectories may overlap during certain time intervals, i.e., there may exist  $T_1, T_2, \xi_i, \xi_j, T_0 \leq T_1 < T_2 \leq T_f, \forall t \in [T_1, T_2], \xi_i(\mathbf{x}, t) = \xi_j(\mathbf{x}, t)$ . The number of Gaussian components of the GMM  $\chi(\mathbf{x}, t)$  is a function of time  $t$  and trajectories  $\Xi$ , denoted as  $F(\Xi, t)$  satisfying  $F(\Xi, t) \leq K, \forall t \in [T_0, T_f]$ . Based on the definition of the path cost in parameter space  $\mathcal{X}$  as outlined in Sec. III, we denote  $|\xi_i(\mathbf{x}, t)| \triangleq \sup_{n \in \mathbb{N}, T_0 \leq t_0 < \dots < t_n = T_f} \sum_{i=1}^n W_2(\xi_i(\mathbf{x}, t_i), \xi_i(\mathbf{x}, t_{i-1}))$  as the transport cost along a PDF trajectory  $\xi_i(\mathbf{x}, t), t \in [T_0, T_f]$ . The optimization problem (1) can be rewritten as:

$$\min_{K, \Lambda, \Xi} \sum_{i=1}^K \lambda_i |\xi_i(\mathbf{x}, t)| \quad (16)$$

$$\text{s.t. } \varrho_{T_0} = \sum_{i=1}^K \lambda_i \xi_i(\mathbf{x}, T_0), \quad (16a)$$

$$\varrho_{T_f} = \sum_{i=1}^K \lambda_i \xi_i(\mathbf{x}, T_f), \quad (16b)$$

$$\xi_i(\mathbf{x}, T_0) \in \{g_{T_0}^1, \dots, g_{T_0}^{N_1}\}, \forall i \in \mathcal{K}, \quad (16c)$$

$$\xi_i(\mathbf{x}, T_f) \in \{g_{T_f}^1, \dots, g_{T_f}^{N_2}\}, \forall i \in \mathcal{K}, \quad (16d)$$

$$\xi_i(\mathbf{x}, t) \in \mathcal{G}, \forall i \in \mathcal{K}, \forall t \in [T_0, T_f], \quad (16e)$$

$$\sum_{i=1}^K \lambda_i = 1, \quad (16f)$$

$$R_\alpha(\xi_i(\mathbf{x}, t)) \leq \delta, \forall t \in [T_0, T_f], \forall i \in \mathcal{K}, \quad (16g)$$

$$K \leq N, \quad (16h)$$

where  $\mathcal{K} = \{1, \dots, K\}$  represents the index set of PDF trajectories,  $\mathcal{G}$  denotes the space of 2-dimensional Gaussian distributions as defined in Sec. III, and (16g) represents the collision avoidance constraint as detailed in Sec. III-B.

The Gaussian roadmap  $G = (V, E)$  constructed in Sec. III with  $n$  nodes  $v_1, \dots, v_n$  and the set of Gaussian components of the swarm initial and target GMMs can be utilized to generate PDF transport trajectories (Line 1-2). Through employing graph search, the optimal trajectory and the corresponding transport cost  $\mathcal{L}(g_{T_0}^i, g_{T_f}^j)$  between each pair of Gaussian distributions ( $g_{T_0}^i, g_{T_f}^j$ ) can be calculated, where  $g_{T_0}^i$  and  $g_{T_f}^j$  represent the  $i$ th and  $j$ th Gaussian components

---

### Algorithm 2: SwarmPRM Algorithm

---

**Input:**  $\varrho_{T_0}$  : the initial GMM,  $\varrho_{T_f}$  : the target GMM,  $\mathcal{Q}$  : the initial positions of swarm robots,  $\mathcal{O}$  : the environmental obstacles

**Output:**  $\mathcal{T}$  : the trajectories of swarm robots

- 1: Obtain the set of Gaussian components  $\Gamma_{T_0}, \Gamma_{T_f}$  of initial and target GMM  $\varrho_{T_0}$  and  $\varrho_{T_f}$
  - 2:  $G = \text{ROADMAPCONSTRUCTION}(n, r_n, \mathcal{O}, \Gamma_{T_0} \cup \Gamma_{T_f})$
  - 3: **for all**  $g_{T_0}^i \in \Gamma_{T_0}$  **do**
  - 4:   **for all**  $g_{T_f}^j \in \Gamma_{T_f}$  **do**
  - 5:     Compute the shortest path from  $g_{T_0}^i$  to  $g_{T_f}^j$  on graph  $G$  using graph search
  - 6:     Compute the optimal transport cost  $\mathcal{L}(g_{T_0}^i, g_{T_f}^j)$
  - 7:   **end for**
  - 8: **end for**
  - 9: Obtain  $\Psi^*$  by solving the LP in (17)
  - 10: Compute  $\mathcal{T}$  from  $\mathcal{Q}$  and  $\Psi^*$  by solving (20)
- 

of  $\varrho_{T_0}$  and  $\varrho_{T_f}$ , respectively (Line 3-8). We can generate the optimal macroscopic GMM trajectories through linear programming (LP) (Line 9)

$$\Psi^* = \arg \min_{\Psi} \sum_{i,j} \Psi(i, j) \mathcal{L}(g_{T_0}^i, g_{T_f}^j), \quad (17)$$

where  $i = 1, \dots, N_1, j = 1, \dots, N_2$ , and the transport policy  $\Psi$  can be written as an  $N_1 \times N_2$  matrix, each element  $\Psi(i, j)$  representing the weight allocated to the trajectory starting at  $g_{T_0}^i$  and ending at  $g_{T_f}^j$ , satisfying

$$\forall j \in \{1, \dots, N_2\}, \sum_{i=1}^{N_1} \Psi(i, j) = \omega_{T_f}^j, \quad (18)$$

$$\forall i \in \{1, \dots, N_1\}, \sum_{j=1}^{N_2} \Psi(i, j) = \omega_{T_0}^i. \quad (19)$$

**Theorem 2.** *The solution (17) is asymptotically optimal for the optimization problem (16).*

*Proof.* The proof will be detailed in Appendix III.  $\square$

### B. Microscopic Motion Planning

Upon determining the optimal evolution of the macroscopic state, represented by the time-varying GMM, each robot can utilize it to compute a local optimal control law and the corresponding collision-free trajectory from the initial position to the target area (Line 10). A centralized artificial potential field (APF) approach is adopted to compute the microscopic robot control inputs for all  $N$  robots,

$$\mathbf{u}_i = -\frac{\partial(w_1 U_{att} + w_2 U_{rep})}{\partial \mathbf{u}_i}, i = 1, \dots, N, \quad (20)$$

where  $U_{att}, U_{rep}$  represent the attractive and repulsive potentials, respectively, and  $w_1, w_2$  are pre-defined weights representing the desired tradeoff between attractive and repulsive objectives. The detailed implementation of the APF approach can be found in [10].

## V. SIMULATION RESULTS

This section verifies the effectiveness and risk awareness of the proposed SwarmPRM approach via several simulations. First, two representative scenarios are generated to demonstrate the validity of the proposed approach both qualitatively and quantitatively. Subsequently, the effectiveness of the risk measure CVaR on collision avoidance is evaluated.

### A. Simulation Setup

In each simulation scenario, the swarm robotic system navigates from a given initial distribution  $\varrho_{T_0} = \sum_{i=1}^{N_1} \omega_{T_0}^i g_{T_0}^i$  to a desired distribution  $\varrho_{T_f} = \sum_{j=1}^{N_2} \omega_{T_f}^j g_{T_f}^j$  while avoiding collisions with obstacles in  $\mathcal{W} = [0, W] \times [0, H]$ , where  $W = 200\text{m}$ ,  $H = 160\text{m}$ ,  $N_1 = 4$ ,  $N_2 = 3$ . The effectiveness of our SwarmPRM approach is evaluated on four swarm robotic systems comprised of  $N = 20, 40, 100, 500$  mobile robots, respectively. Each robot is of circular shape with a radius of  $r = 0.2\text{m}$  and is characterized by single-integrator dynamics

$$\dot{\mathbf{x}}_i(t) = \mathbf{u}_i(t), \mathbf{x}_i(T_0) = \mathbf{x}_{i_0}, \forall i \in \{1, \dots, N\}, \quad (21)$$

where  $\mathbf{x}_i = [x_i, y_i]^T$  denotes the robot position,  $x_i$  and  $y_i$  are the robot  $xy$ -coordinates in inertial frame, and the control input  $\mathbf{u}_i$  is a vector of linear velocities in the  $x$ - and  $y$ -directions. When constructing the Gaussian roadmap  $G$ , we set  $\sigma_{lb}, \sigma_{ub}, \rho_{ub}, \rho_{lb}$  to be 3, 12,  $-0.9, 0.9$ , respectively, the number of samples  $n = 500$ , and the connection radius  $r_n > 2(\frac{6}{5})^{\frac{1}{5}} (\frac{\mu(\mathcal{X}_{free})}{\mu(\mathcal{B})})^{\frac{1}{5}} (\frac{\log(n)}{n})^{\frac{1}{5}}$  to ensure asymptotic optimality of our approach (Appendix II). The simulations are implemented using MATLAB code, and executed on a laptop with Intel Core i7-1065G7 CPU@1.30GHz and 16GB RAM. In practical implementation, to avoid excessively high local densities in the swarm macroscopic state  $\chi(\mathbf{x}, t)$  which adds difficulty to microscopic planning, we add extra constraints to the LP in (17), which can be modeled as a minimum-cost flow problem.

### B. Performance Comparison

Two representative two-dimensional complex environments are designed to evaluate the performance of our approach both qualitatively and quantitatively, as well as three state-of-the-art sampling-based or hierarchical motion planning methods, including multi-robots formation control [8], discrete RRT\* [18], and adaptive distributed optimal control [10], denoted as Formation control, dRRT\*, and ADOC, respectively. In each environment, swarm robotic systems consisting of  $N = 20, 40, 100, 500$  robots are required to move from initial configurations to target areas. The performance can be assessed by the computational time  $T_{sol}$  and the average cost-to-go

$$\bar{D} = \frac{1}{N} \sum_{i=1}^N \sum_{\tau=0}^{\kappa-1} \|\mathbf{x}_i[T_0 + (\tau+1)\Delta t] - \mathbf{x}_i(T_0 + \tau\Delta t)\|_2, \quad (22)$$

where  $\kappa = \frac{T_f - T_0}{\Delta t}$ .

TABLE I: Simulation Results in Environment I

$N$	Metrics	SwarmPRM	Formation control	dRRT*	ADOC
20	$T_{sol}(\text{min})$	<b>7.1</b>	34.5	115.5	12.8
	$\bar{D}(\text{m})$	250.3	296.0	<b>242.4</b>	271.0
40	$T_{sol}(\text{min})$	<b>7.8</b>	37.3	120.0	12.9
	$\bar{D}(\text{m})$	<b>253.4</b>	309.2	412.8	271.1
100	$T_{sol}(\text{min})$	<b>8.4</b>	47.3	–	13.8
	$\bar{D}(\text{m})$	<b>254.0</b>	320.3	–	272.8
500	$T_{sol}(\text{min})$	<b>14.6</b>	303.5	–	21.7
	$\bar{D}(\text{m})$	<b>255.7</b>	327.9	–	274.1

1) *Environment I*: We consider an environment containing 3 nonconvex obstacles, which is presented in the left column of Fig. 2. Our SwarmPRM approach demonstrates significantly shorter computational time  $T_{sol}$  in comparison with Formation control and dRRT\*, as illustrated in Tab. I, showcasing remarkable scalability and computational efficiency. As for the Formation control approach, the local motion planning requires solving a distributed nonlinear optimization for each robot at high frequency to avoid collisions, and the overall computational time increases rapidly with the number of robots in the swarm. On the other hand, the dRRT\* approach can find solutions for swarm robotic systems consisting of up to around 40 robots in environment I, but for swarm robotic systems comprising  $N = 100, 500$  robots, dRRT\* cannot find a solution within 2 hours due to the exponential growth of the search space. Furthermore, our SwarmPRM approach outperforms Formation control in terms of the average cost-to-goal  $\bar{D}$  across all scenarios, demonstrating the asymptotic optimality property of SwarmPRM under mild assumptions. When compared to dRRT\*, our approach yields solutions with lower  $\bar{D}$  when  $N = 40$ , as dRRT\* faces substantial computational burden and cannot find better solutions within the allotted two-hour computational time.

Our SwarmPRM approach surpasses ADOC on both metrics,  $T_{sol}$  and  $\bar{D}$ , showcasing the efficacy of the sampling-based planning method at the macroscopic stage to plan trajectories with lower costs under shorter computational time. The left column of Fig. 2 shows the trajectories of the swarm robotic system comprising 500 robots using SwarmPRM, Formation control, ADOC, respectively. The SwarmPRM and ADOC allow splitting and merging of robots, while the Formation control requires the maintenance of a formation for all robots in the swarm. Furthermore, all approaches successfully plan a collision-free trajectory for each robot with respect to all obstacles and other robots.

2) *Environment II*: In environment II, 10 obstacles are randomly distributed, as depicted in the right column of Fig. 2. The results, as shown in Tab. II, show similar trends to those discussed in Sec. V-B.1. Illustrations of the trajectories of a swarm robotic system comprising 500 robots using SwarmPRM, Formation control, and ADOC are provided in the right column of Fig. 2. The macroscopic GMM trajectory planned by SwarmPRM can cross "narrow passages", leading to lower average-cost-to-goal  $\bar{D}$  compared to ADOC.

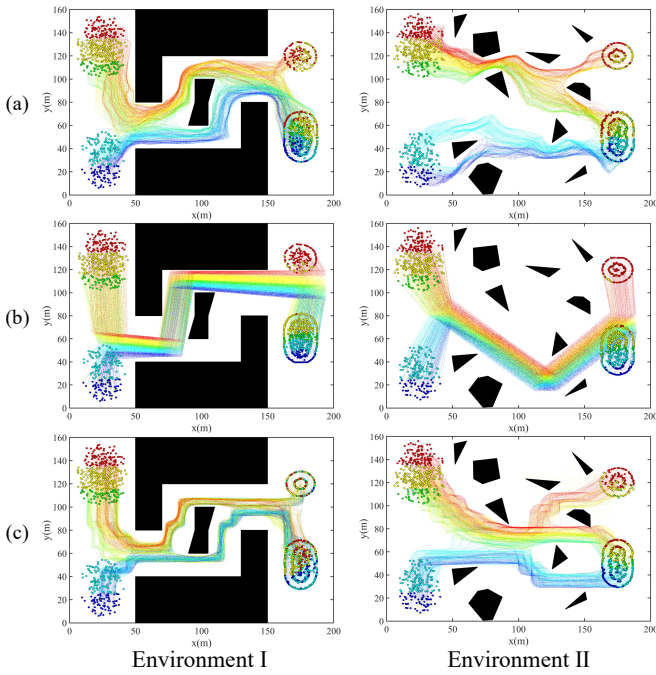


Fig. 2: **Trajectory comparison in environment I and II.** The trajectories of the swarm robotic system comprised of  $N = 500$  robots obtained by (a) SwarmPRM, (b) Formation control, and (c) ADOC, for the same set of initial positions in each environment. The initial and final positions are represented by coloured circles on the left and right sides of each figure, respectively, while the obstacles are depicted in black colour.

TABLE II: Simulation Results in Environment II

$N$	Metrics	SwarmPRM	Formation control	dRRT*	ADOC
20	$T_{sol}(\text{min})$	<b>6.8</b>	26.2	115.6	10.6
	$\bar{D}(\text{m})$	<b>192.3</b>	271.2	208.2	205.8
40	$T_{sol}(\text{min})$	<b>7.0</b>	38.5	120.0	10.9
	$\bar{D}(\text{m})$	<b>192.7</b>	272.8	289	206.0
100	$T_{sol}(\text{min})$	<b>7.6</b>	54.1	—	11.5
	$\bar{D}(\text{m})$	<b>193.1</b>	280.4	—	206.8
500	$T_{sol}(\text{min})$	<b>9.2</b>	271.2	—	25.3
	$\bar{D}(\text{m})$	<b>193.5</b>	280.7	—	208.5

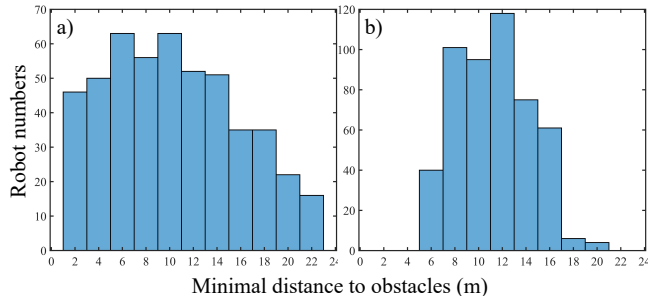


Fig. 3: (a) and (b) illustrate the minimal distance from each robot to the set of obstacles along the overall trajectory, with risk parameter  $\alpha = 0.3$  and  $0.1$ , respectively.

### C. Evaluation of the Risk Measure CVaR

To demonstrate the effectiveness and risk awareness of the risk measure CVaR, we set the risk parameter  $\alpha$  to be 0.3 and 0.1, and during the construction of the Gaussian roadmap, the functions INFREE and COLLISIONFREE perform collision detection based on (15), ensuring the conditional expectation of the SDF within the 30% and 10% worst-case quantiles falls in the safe region, respectively. We set the number of robots in the swarm to be 500, and calculate the minimal distance from each robot to the set of obstacles along the entire trajectory under different values of the risk parameter  $\alpha$ . As Fig. 3 shows, a smaller risk parameter  $\alpha$  leads to a higher percentage of robots positioned further away from the obstacles, affirming the effectiveness and risk awareness of employing CVaR for collision avoidance. Furthermore, we can regulate the proximity of the robot swarm to obstacles by adjusting the risk parameter  $\alpha$ .

## VI. CONCLUSION

We develop the SwarmPRM algorithm for motion planning of swarm robotic systems. At the macroscopic level, a risk-aware Gaussian roadmap is constructed where each node represents a distinct Gaussian distribution and CVaR is utilized for collision checking. The Gaussian roadmap aids in generating the macroscopic time-varying PDF in Wasserstein–GMM space, which is asymptotically optimal under mild assumptions. Simulation results show that SwarmPRM significantly outperforms other state-of-the-art approaches in aspects of computational efficiency and average travelling distance.

## REFERENCES

- [1] K. McGuire, C. De Wagter, K. Tuyls, H. Kappen, and G. C. de Croon, “Minimal navigation solution for a swarm of tiny flying robots to explore an unknown environment,” *Science Robotics*, vol. 4, no. 35, p. eaaw9710, 2019.
- [2] D. S. Drew, “Multi-agent systems for search and rescue applications,” *Current Robotics Reports*, vol. 2, pp. 189–200, 2021.
- [3] F. Schilling, J. Lecoœur, F. Schiano, and D. Floreano, “Learning vision-based flight in drone swarms by imitation,” *IEEE Robotics and Automation Letters*, vol. 4, no. 4, pp. 4523–4530, 2019.
- [4] E. Soria, F. Schiano, and D. Floreano, “Predictive control of aerial swarms in cluttered environments,” *Nature Machine Intelligence*, vol. 3, no. 6, pp. 545–554, 2021.
- [5] M. A. Pereira, A. D. Saravanos, O. So, and E. A. Theodorou, “Decentralized safe multi-agent stochastic optimal control using deep fbsdes and admm,” *arXiv preprint arXiv:2202.10658*, 2022.
- [6] T. Zheng, Q. Han, and H. Lin, “Transporting robotic swarms via mean-field feedback control,” *IEEE Transactions on Automatic Control*, vol. 67, no. 8, pp. 4170–4177, 2021.
- [7] S. Ma, M. Hou, X. Ye, and H. Zhou, “High-dimensional optimal density control with wasserstein metric matching,” in *2023 62nd IEEE Conference on Decision and Control (CDC)*. IEEE, 2023, pp. 6813–6818.
- [8] J. Alonso-Mora, S. Baker, and D. Rus, “Multi-robot formation control and object transport in dynamic environments via constrained optimization,” *The International Journal of Robotics Research*, vol. 36, no. 9, pp. 1000–1021, 2017.
- [9] K. Rudd, G. Foderaro, P. Zhu, and S. Ferrari, “A generalized reduced gradient method for the optimal control of very-large-scale robotic systems,” *IEEE transactions on robotics*, vol. 33, no. 5, pp. 1226–1232, 2017.
- [10] P. Zhu, C. Liu, and S. Ferrari, “Adaptive online distributed optimal control of very-large-scale robotic systems,” *IEEE Transactions on Control of Network Systems*, vol. 8, no. 2, pp. 678–689, 2021.



- [11] H. Zhu and J. Alonso-Mora, "Chance-constrained collision avoidance for mavs in dynamic environments," *IEEE Robotics and Automation Letters*, vol. 4, no. 2, pp. 776–783, 2019.
- [12] A. Hakobyan and I. Yang, "Distributionally robust risk map for learning-based motion planning and control: A semidefinite programming approach," *IEEE Transactions on Robotics*, vol. 39, no. 1, pp. 718–737, 2022.
- [13] X. Yang, H. Gao, P. Zhu, and C. Liu, "Risk-aware motion planning for very-large-scale robotics systems using conditional value-at-risk," in *International Conference on Intelligent Robotics and Applications*. Springer, 2023, pp. 513–525.
- [14] P. Artzner, F. Delbaen, J.-M. Eber, and D. Heath, "Coherent measures of risk," *Mathematical finance*, vol. 9, no. 3, pp. 203–228, 1999.
- [15] S. Karaman and E. Frazzoli, "Sampling-based algorithms for optimal motion planning," *The international journal of robotics research*, vol. 30, no. 7, pp. 846–894, 2011.
- [16] M. Čáp, P. Novák, J. Vokřínek, and M. Pěchouček, "Multi-agent rrt: sampling-based planning for quadrotor swarms," in *Proceedings of the 2013 international conference on Autonomous agents and multi-agent systems*, 2013, pp. 1263–1264.
- [17] W. Hönig, J. A. Preiss, T. S. Kumar, G. S. Sukhatme, and N. Ayanian, "Trajectory planning for quadrotor swarms," *IEEE Transactions on Robotics*, vol. 34, no. 4, pp. 856–869, 2018.
- [18] R. Shome, K. Solovey, A. Dobson, D. Halperin, and K. E. Bekris, "drrt\*: Scalable and informed asymptotically-optimal multi-robot motion planning," *Autonomous Robots*, vol. 44, no. 3-4, pp. 443–467, 2020.
- [19] S. LaValle, "Planning algorithms," *Cambridge University Press google scholar*, vol. 2, pp. 3671–3678, 2006.
- [20] L. Janson, B. Ichter, and M. Pavone, "Deterministic sampling-based motion planning: Optimality, complexity, and performance," *The International Journal of Robotics Research*, vol. 37, no. 1, pp. 46–61, 2018.
- [21] Y. Chen, T. T. Georgiou, and A. Tannenbaum, "Optimal transport for gaussian mixture models," *IEEE Access*, vol. 7, pp. 6269–6278, 2018.
- [22] G. Auricchio, F. Bassetti, S. Gualandi, and M. Veneroni, "Computing kantorovich-wasserstein distances on  $d$ -dimensional histograms using  $(d + 1)$ -partite graphs," *Advances in Neural Information Processing Systems*, vol. 31, 2018.
- [23] I. Goodfellow, Y. Bengio, and A. Courville, *Deep learning*. MIT press, 2016.
- [24] H. Gao, P. Wu, Y. Su, K. Zhou, J. Ma, H. Liu, and C. Liu, "Probabilistic visibility-aware trajectory planning for target tracking in cluttered environments," *arXiv preprint arXiv:2306.06363*, 2023.
- [25] R. Bhatia, T. Jain, and Y. Lim, "On the bures–wasserstein distance between positive definite matrices," *Expositiones Mathematicae*, vol. 37, no. 2, pp. 165–191, 2019.
- [26] M. R. Bridson and A. Haeffliger, *Metric spaces of non-positive curvature*. Springer Science & Business Media, 2013, vol. 319.
- [27] L. Janson, E. Schmerling, A. Clark, and M. Pavone, "Fast marching tree: A fast marching sampling-based method for optimal motion planning in many dimensions," *The International journal of robotics research*, vol. 34, no. 7, pp. 883–921, 2015.

## APPENDIX I PROOF OF LEMMA 1

**Lemma 1:** The cost function  $c$  defined based on the Wasserstein metric satisfies: 1) the triangle inequality,  $\forall \mathbf{v}_i, \mathbf{v}_j, \mathbf{v}_k \in \mathcal{X}, c(\mathbf{v}_i, \mathbf{v}_j) + c(\mathbf{v}_j, \mathbf{v}_k) \geq c(\mathbf{v}_i, \mathbf{v}_k)$ , 2) additivity,  $\forall \varphi_1, \varphi_2 : [0, 1] \rightarrow \mathcal{X}, \varphi_1(1) = \varphi_2(0), L(\varphi_1 \varphi_2) = L(\varphi_1) + L(\varphi_2)$ , where  $\varphi_1 \varphi_2$  denotes the concatenation of two paths when  $\varphi_1$  ends at the point at which  $\varphi_2$  begins, and  $L(\varphi) \triangleq \sup_{n \in \mathbb{N}, 0 = \iota_0 < \dots < \iota_n = 1} \sum_{i=1}^n c(\varphi(\iota_i) - \varphi(\iota_{i-1}))$ , and 3) natural relationship with Euclidean distance in the configuration space,  $\exists \hat{\beta}_1, \hat{\beta}_2 \in (0, \infty), \forall \mathbf{v}_i, \mathbf{v}_j \in [0, 1]^5, \hat{\beta}_1 \|\mathbf{v}_i - \mathbf{v}_j\| \leq c(\mathbf{v}_i, \mathbf{v}_j) \leq \hat{\beta}_2 \|\mathbf{v}_i - \mathbf{v}_j\|$ .

*Proof.* The Wasserstein metric between two Gaussian distributions  $g_1 \sim \mathcal{N}(\boldsymbol{\mu}_1, \Sigma_1), g_2 \sim \mathcal{N}(\boldsymbol{\mu}_2, \Sigma_2)$  can be written

as:

$$W_2(g_1, g_2) = [W_{\boldsymbol{\mu}}^2(g_1, g_2) + W_{\Sigma}^2(g_1, g_2)]^{\frac{1}{2}}, \quad (23)$$

where

$$W_{\boldsymbol{\mu}}^2(\varrho_1, \varrho_2) = \|\boldsymbol{\mu}_1 - \boldsymbol{\mu}_2\|_2^2, \quad (24)$$

$$W_{\Sigma}^2(\varrho_1, \varrho_2) = \text{tr} \left[ \Sigma_1 + \Sigma_2 - 2(\Sigma_1^{\frac{1}{2}} \Sigma_2 \Sigma_1^{\frac{1}{2}})^{\frac{1}{2}} \right]. \quad (25)$$

The  $W_{\boldsymbol{\mu}}$  corresponds to the Euclidean distance in a 2-dimensional vector space, and the  $W_{\Sigma}$  is a metric in the space of  $2 \times 2$  positive definite matrixes [25], both satisfying the property of positivity, symmetry, and triangle inequality in their respective spaces, and thus the Wasserstein metric in the space of Gaussian distributions  $\mathcal{G}$  is also a cost metric. Because of the fact that 1) the mapping  $h$  and  $h^{-1}$  between  $\mathcal{G}$  and  $\mathcal{X}$  is a bijection, and 2) the cost function  $c$  satisfying  $\forall \mathbf{v}_i, \mathbf{v}_j \in \mathcal{X}, c(\mathbf{v}_i, \mathbf{v}_j) = W_2(g_i, g_j)$ , where  $g_i = h(\mathbf{v}_i) \in \mathcal{G}, g_j = h(\mathbf{v}_j) \in \mathcal{G}$  is defined based on the Wasserstein metric, we reach the conclusion that  $(\mathcal{X}, c)$  is a metric space, and 1) the triangle inequality, 2) additivity [26], are both satisfied.

We then prove 3), the natural relationship with the Euclidean distance. The covariance matrix  $\Sigma_1$  and  $\Sigma_2$  can be written as

$$\Sigma_1 = \begin{bmatrix} a_1^2 & \rho_1 a_1 b_1 \\ \rho_1 a_1 b_1 & b_1^2 \end{bmatrix},$$

$$\Sigma_2 = \begin{bmatrix} a_2^2 & \rho_2 a_2 b_2 \\ \rho_2 a_2 b_2 & b_2^2 \end{bmatrix},$$

$$0 < \sigma_{lb} \leq a_1, a_2, b_1, b_2 \leq \sigma_{ub}, \quad (26)$$

$$-1 < \rho_{lb} \leq \rho_1, \rho_2 \leq \rho_{ub} < 1. \quad (27)$$

We can represent  $W_{\Sigma}^2(g_1, g_2)$  using  $a_1, a_2, b_1, b_2, \rho_1, \rho_2$ ,

$$W_{\Sigma}^2(g_1, g_2) = a_1^2 + a_2^2 + b_1^2 + b_2^2 - \sqrt{2} \left[ (z_1 - z_2)^{\frac{1}{2}} + (z_1 + z_2)^{\frac{1}{2}} \right], \quad (28)$$

$$z_1 = a_1^2 a_2^2 + b_1^2 b_2^2 + 2a_1 a_2 b_1 b_2 \rho_1 \rho_2, \quad (29)$$

$$z_2 = \sqrt{z_1 - 4a_1^2 a_2^2 b_1^2 b_2^2 (1 - \rho_1^2)(1 - \rho_2^2)}. \quad (30)$$

The Eq. (28) can be calculated based on Eq. (3) and the fact that  $\text{tr}[(\Sigma_1^{\frac{1}{2}} \Sigma_2 \Sigma_1^{\frac{1}{2}})^{\frac{1}{2}}] = \text{tr}[(\Sigma_1 \Sigma_2)^{\frac{1}{2}}] = \sum_i \sqrt{\hat{\lambda}_i(\Sigma_1 \Sigma_2)}$ , where  $\hat{\lambda}_i(\cdot)$  represents the  $i$ th largest eigenvalue of a positive definite matrix.

We first consider the lower bound of  $W_{\Sigma}^2(g_1, g_2)$ ,

$$(z_1 + z_2)^{\frac{1}{2}} + (z_1 - z_2)^{\frac{1}{2}} = \sqrt{2z_1 + 2\sqrt{z_1^2 - z_2^2}} = \left[ 2a_1^2 a_2^2 + 2b_1^2 b_2^2 + 4a_1 a_2 b_1 b_2 \rho_1 \rho_2 + 4a_1 a_2 b_1 b_2 \sqrt{(1 - \rho_1^2)(1 - \rho_2^2)} \right]^{\frac{1}{2}}. \quad (31)$$

Denote  $\delta = \rho_1 - \rho_2$ . Then we have

$$\rho_1 \rho_2 + \sqrt{(1 - \rho_1^2)(1 - \rho_2^2)} \leq \rho_1 \rho_2 + \frac{2 - \rho_1^2 - \rho_2^2}{2} = 1 - \frac{\delta^2}{2}, \quad (32)$$

$$W_{\Sigma}^2(g_1, g_2) \geq a_1^2 + a_2^2 + b_1^2 + b_2^2 - 2\sqrt{a_1^2 a_2^2 + b_1^2 b_2^2 + 2a_1 a_2 b_1 b_2 (1 - \frac{\delta^2}{2})}. \quad (33)$$

We can prove the following conclusion: if  $\beta_1 \leq \frac{\sigma_{ub}^4}{2\sigma_{ub}^2 + 1}$ , then  $W_{\Sigma}^2(g_1, g_2) \geq \beta_1[(a_1 - a_2)^2 + (b_1 - b_2)^2 + (\rho_1 - \rho_2)^2]$ , through the following steps:

$$a_1 a_2 b_1 b_2 \geq \frac{\beta_1^2 \delta^2}{4} + \beta_1 \sqrt{(a_1 a_2 + b_1 b_2)^2 - a_1 a_2 b_1 b_2 \delta^2}, \quad (34)$$

$$\frac{\beta_1^2 \delta^4}{4} - a_1 a_2 b_1 b_2 \delta^2 + \beta_1 \delta^2 \sqrt{(a_1 a_2 + b_1 b_2)^2 - a_1 a_2 b_1 b_2 \delta^2} \leq 0, \quad (35)$$

$$a_1 a_2 + b_1 b_2 \geq \frac{\beta_1 \delta^2}{2} + \sqrt{(a_1 a_2 + b_1 b_2)^2 - a_1 a_2 b_1 b_2 \delta^2}, \quad (36)$$

$$W_{\Sigma}^2(g_1, g_2) \geq (a_1 - a_2)^2 + (b_1 - b_2)^2 + \beta_1 \delta^2 \geq \beta_1[(a_1 - a_2)^2 + (b_1 - b_2)^2 + (\rho_1 - \rho_2)^2]. \quad (37)$$

Next we consider the upper bound of  $W_{\Sigma}^2(g_1, g_2)$ . The Eq. (28) can be rewritten as

$$W_{\Sigma}^2(g_1, g_2) = (a_1 - a_2)^2 + (b_1 - b_2)^2 + 2 \left[ a_1 a_2 + b_1 b_2 - \sqrt{a_1^2 a_2^2 + b_1^2 b_2^2 + 2a_1 a_2 b_1 b_2 (\rho_1 \rho_2 + \sqrt{(1 - \rho_1^2)(1 - \rho_2^2)})} \right]. \quad (38)$$

Denote  $\frac{[a_1^2 a_2^2 + b_1^2 b_2^2 + 2a_1 a_2 b_1 b_2 (\rho_1 \rho_2 + \sqrt{(1 - \rho_1^2)(1 - \rho_2^2)})]^{\frac{1}{2}}}{a_1 a_2 + b_1 b_2 - z_3}$  as  $z_3$ , and we have

$$\frac{a_1 a_2 + b_1 b_2 - z_3}{(\rho_1 - \rho_2)^2} = \frac{2a_1 a_2 b_1 b_2 (1 - \rho_1 \rho_2 - \sqrt{(1 - \rho_1^2)(1 - \rho_2^2)})}{(a_1 a_2 + b_1 b_2 + z_3)(\rho_1 - \rho_2)^2}. \quad (39)$$

Since  $-1 < \rho_{lb} \leq \rho_1, \rho_2 \leq \rho_{ub} < 1$ , and  $a_1, b_1, a_2, b_2 \leq \sigma_{ub}$ , the following two inequalities holds:

$$\frac{2(1 - \rho_1 \rho_2 - \sqrt{(1 - \rho_1^2)(1 - \rho_2^2)})}{(\rho_1 - \rho_2)^2} \leq \frac{1}{1 - \max(\rho_{ub}^2, \rho_{lb}^2)}, \quad (40)$$

$$\begin{aligned} \frac{a_1 a_2 b_1 b_2}{a_1 a_2 + b_1 b_2 + z_3} &= \frac{1}{\frac{1}{a_1 a_2} + \frac{1}{b_1 b_2} + \frac{z_3}{a_1 a_2 b_1 b_2}} \\ &\leq \frac{1}{\frac{2}{\sigma_{ub}^2} + \sqrt{\frac{4 - 4 \max(\rho_{ub}^2, \rho_{lb}^2)}{\sigma_{ub}^4}}} \\ &= \frac{\sigma_{ub}^2}{2 + 2\sqrt{1 - \max(\rho_{ub}^2, \rho_{lb}^2)}}. \end{aligned} \quad (41)$$

Denote  $\max(\rho_{ub}^2, \rho_{lb}^2)$  as  $\hat{\rho}^2$ . The upper bound of Eq. (39) can be written by the product of the (40) and (41), and the upper bound of  $W_{\Sigma}^2(g_1, g_2)$  is

$$W_{\Sigma}^2(g_1, g_2) \leq (a_1 - a_2)^2 + (b_1 - b_2)^2 + (\rho_1 - \rho_2)^2 \frac{\sigma_{ub}^2}{(1 - \hat{\rho}^2)(1 + \sqrt{1 - \hat{\rho}^2})}, \quad (42)$$

and the corresponding  $\hat{\beta}_2$  can be found.  $\square$

## APPENDIX II PROOF OF THEOREM 1

**Theorem 1:** The Alg. 1 is asymptotically optimal for planning the PDF transport trajectory between any two Gaussian distributions.

*Proof.* We've demonstrated that the cost function  $c$  in parameter space  $\mathcal{X}$  satisfies the triangle inequality, additivity, and the natural relationship with the Euclidean distance. The natural relationship enables the Lebesgue measure of the unit cost-ball  $\mathcal{B}$ , denoted as  $\mu(\mathcal{B})$  to be contained in  $(0, +\infty)$  [27]. Building upon the results in [15, 27], we establish the asymptotic optimality of Alg. 1 by employing the random sampling strategy in the five-dimensional parameter space  $\mathcal{X}$ , and setting the connection radius  $r_n$  to be any value greater than  $2(\frac{6}{5})^{\frac{1}{5}} (\frac{\mu(\mathcal{X}_{free})}{\mu(\mathcal{B})})^{\frac{1}{5}} (\frac{\log(n)}{n})^{\frac{1}{5}}$ , where  $\mu(\mathcal{X}_{free})$  denotes the Lebesgue measure of the obstacle-free space. According to the proof in [20], the Alg. 1 is asymptotic optimal if we utilize a deterministic sampling sequence in five dimensions with  $l_2$ -dispersion upper bounded by  $\gamma n^{-\frac{1}{5}}$ , and set  $r_n$  satisfying  $n^{\frac{1}{5}} r_n \rightarrow \infty$ .  $\square$

## APPENDIX III PROOF OF THEOREM 2

**Theorem 2:** The solution (17) is asymptotically optimal for the optimization problem (16).

*Proof.* According to Theorem 1, for each pair of Gaussian distributions  $(g_{T_0}^i, g_{T_f}^j)$ , the Alg. 1 can return a collision-free trajectory  $g_{i,j}^n$  from a PRM graph consisting of  $n$  nodes satisfying  $\lim_{n \rightarrow +\infty} |g_{i,j}^n| = |g_{i,j}^*|$ , where  $g_{i,j}^*$  represents the optimal transport trajectory, and  $|\cdot|$  denotes the cost of a PDF trajectory calculated using the Wasserstein metric. The minimum of the objective function in (16) is  $\sum_{i,j} \Psi^*(i, j) |g_{i,j}^*|$ , and  $\lim_{n \rightarrow +\infty} \sum_{i,j} \Psi^*(i, j) |g_{i,j}^n| = \sum_{i,j} \Psi^*(i, j) |g_{i,j}^*|$ , where  $\{g_{1,1}^n, \dots, g_{N_1, N_2}^n\}$  is the set of Gaussian trajectories planned by Alg. 1. Denote the solution to (17) as  $\Psi^n(i, j)$ , and the following inequality holds

$$\sum_{i,j} \Psi^*(i, j) |g_{i,j}^*| \leq \sum_{i,j} \Psi^n(i, j) |g_{i,j}^n| \leq \sum_{i,j} \Psi^*(i, j) |g_{i,j}^n|. \quad (43)$$

We reach the conclusion that

$$\lim_{n \rightarrow +\infty} \sum_{i,j} \Psi^n(i, j) |g_{i,j}^n| = \sum_{i,j} \Psi^*(i, j) |g_{i,j}^*|, \quad (44)$$

and therefore the asymptotic optimality is established. Each non-zero element  $\Psi^n(i, j)$  corresponds to a Gaussian trajectory from  $g_{T_0}^i$  to  $g_{T_f}^j$  with weight  $\Psi^n(i, j)$ .  $\square$